Current-cycle iterative learning control for high-precision position tracking of piezoelectric actuator system via active disturbance rejection control for hysteresis compensation

Article (Accepted Version)

Current-cycle Iterative Learning Control for High-precision Position Tracking of Piezoelectric Actuator System via Active Disturbance Rejection Control for Hysteresis Compensation

Deqing Huang, *Member*, *IEEE*, Da Min, Yupei Jian, and Yanan Li, *Member*, *IEEE*

***Abstract*—As a typical smart structure, piezoelectric actuator (PEA) is an essential constituent component in piezoelectric-driven positioning stages. Nevertheless, the positioning precision is severely degraded by its innate rate-dependent hysteretic nonlinearity. In this paper, an innovative control method which combines active disturbance rejection control (ADRC) and current-cycle iterative learning control (CILC) is proposed by constructing PEA as a second-order disturbance-based (SODB) structure to handle both hysteretic nonlinearities and dynamic uncertainties of PEA. The proposed method differs from the prevalent model-inverse solution in hysteresis compensation, where the control performance of the latter extremely relies on the accurateness of the hysteretic model while the former does not require a mathematical model of hysteresis since it is considered as a general disturbance and eliminated. Compared with the existing hysteresis compensation via pure ADRC method, the proposed method has improved robustness by incorporating an additional ILC loop to ADRC. Comparative experimentations are executed on a PEA system and results imply that the proposed approach has better control performance than pure proportional-integral (PI) control and ADRC.**

***Index Terms*—active disturbance rejection control (ADRC), hysteresis compensation, current-cycle iterative learning control (CILC), tracking precision, piezoelectric actuator (PEA).**

I. Introduction

PRECISE motion control of nano-positioning stages has been extensively studied for decades and has become an indispensable technology in areas of engineering and manufacturing. Piezoelectric actuator (PEA) as a representative smart structure has the merits of high resolution, fast response and nanometer control precision [1]. It is an essential constituent component in multifarious implementation of high-precision tracking control, used as the probe in the scanning micromirror [2], employed in active vibration damping of railway car bodies [3], and so on. Nevertheless, the inherent rate-dependent hysteretic nonlinearity [4] of PEA includes a class of typical input and output uncertainties and it severely restricts the control performance of motion systems, even resulting system instability. Therefore, it is crucial to inhibit the hysteretic characteristic in piezoelectric-driven precise motion systems.

Considerable studies have been conducted in solving the tracking problem of PEA. Multitudinous control methods have been proposed, for instance, sliding mode control [5], [6], adaptive control [7], H_∞ control [8], as well as proportional-integral-derivative (PID) control [9]. The main idea of aforementioned approaches is the alleged hysteresis model-based strategy where the hysteretic effect of PEA is cancelled by its direct inverse model. Thus the model of the hysteresis is needed in order to obtain its inverse. Abundant literature concentrates on modeling of the hysteresis phenomenon involving neural network model [10], modified Prandtl-Ishlinskii (MPI) model [11], Bouc-Wen model [12], and so on. Note that the aforementioned hysteresis model-based approach highly depends on the accurateness of an exhaustive hysteresis model. Yet, multi-valued mapping and memorability of PEA [13] lead to the identification of an accurate hysteresis model time-consuming and there always exists modelling error to some extent. Furthermore, the calculation of the inverse hysteresis model is always difficult and troublesome.

Active disturbance rejection control (ADRC) scheme has been proved to be an effective solution in system control and disturbance/uncertainty estimation since it was presented in [14]. It also exhibits prospect performance and tremendous superiorities in high-precision motion systems. ADRC does not need a detailed hysteresis model as it is regarded as a general disturbance and eliminated. Many research works have been made by using the ADRC approach to compensate for the hysteresis [15]–[18]. As a matter of fact, although the ADRC can achieve acceptable accuracy in tracking periodic low-frequency reference, the control performance will be degraded severely in high-frequency tracking tasks owing to a connatural mismatch between the estimation of disturbance and its actual value which limits the compensation of the hysteresis.

The intention of this paper is to exploit a pragmatic itera-

Manuscript received September 24, 2018; revised May 14, 2019, July 12, 2019, and August 10, 2019; accepted September 30, 2019. This work was supported by the National Natural Science Foundation of China under Grant 61773323 and Grant 61603316. *(Corresponding author: Yanan Li.)*

Deqing Huang, and Da Min are with the Institute of Systems Science and Technology, Southwest Jiaotong University, Chengdu 610031, China (e-mail: elehd@home.swjtu.edu.cn; dmin@my.swjtu.edu.cn).

Yupei Jian is with the Department of Mechanical Engineering, University of Auckland, Auckland 1010, N.Z. (e-mail: yjia597@aucklanduni.ac.nz).

Yanan Li is with the Department of Engineering and Design, University of Sussex, Sussex BN1 9RH, U.K. (e-mail: hit.li.yn@gmail.com).

tive learning control (ILC) methodology to further enhance the tracking performances of PEA systems when the rate-dependent hysteretic nonlinearity is compensated for incompletely via ADRC. The idea of using ILC to compensate for tracking errors in PEA has been implemented in many existing works. In [19], experiments have been implemented to verify that using ILC to eliminate the repetitive tracking error is effective. In [20], an ILC based model-inverse method is explored for PEA systems without considering the hysteresis nonlinearity, and the controller design is simplified by linearizing the hysteresis. In [21], a Hammerstein model is adopted to describe the hysteretic characteristics and precise tracking tasks of PEA are handled via combining ILC and direct inverse model for hysteresis compensation. In [22], remarkable tracking performance is obtained by adding a pure ILC loop to a feedback control loop to compose the current-cycle ILC (CILC), and gain scheduling is used to handle the repetitive tracking error and non-repetitive disturbances.

Nevertheless, few research works have united ADRC with ILC to address hysteresis compensation and high-performance position tracking task of PEA. The advantage of adopting such a novel control scheme is: while the hysteretic nonlinearity of the PEA is considered as a general disturbance and eliminated through applying ADRC so that the detailed hysteresis model and its inversion are no longer needed, the tracking error can be reduced promptly via ILC. More specifically, in this paper, by regarding the hysteretic nonlinearity and dynamic uncertainties as a general disturbance, a second-order disturbance-based (SODB) model which is redeveloped from the integrated dynamic model is adopted to represent the complex relationships between the control input and the displacement output of the PEA. Then, a linear extended state observer (LESO) is used to estimate the general disturbance so that the SODB model of the PEA comes close to the equivalent double integral (EDI) model.

For the controller design part, the hysteresis nonlinearity is first compensated for by using the estimation of the disturbance from LESO. Then, the compensated EDI structure is controlled by choosing a pure PI controller and a sampled-data CILC law is designed and executed to address the influence caused by the estimation error which degrades the tracking performances. The convergence of the entire control system is derived rigorously in the frequency domain. Different from those prevailing model-inverse methods for hysteresis compensation, which extremely depends on the accurateness of an exhaustive hysteresis model, the proposed method is independent of the mathematical model of hysteresis since the hysteresis is considered as a general disturbance and eliminated. It provides more robustness than the existing pure ADRC solution for hysteresis compensation by incorporating an additional ILC loop to ADRC. In addition, the tracking precision is improved considerably within 6 iterations in the sense of maximal absolute error (MAE), relative error (RE), and root mean square error (RMSE) of the output tracking, which is demonstrated by comparative experiments.

Overall, the innovation of this paper is that the proposed creative control scheme, which combines ADRC and CILC, concentrates on effectiveness of compensation without using a hysteresis model and feasibility of implementation in practical applications. On the other hand, as far as the authors know, a combined ADRC and CILC scheme has not been realized before. It is the first effort which deals with the high-precision positioning tasks of PEA systems by means of combining ADRC and CILC, where the former is aimed at compensating for hysteresis and boosting the learning convergence by regarding the nonlinearity of hysteresis as disturbance while the latter is conducted to further enhance the control performances and robustness of the whole control system via adding a CILC loop when ADRC compensates for the hysteresis incompletely. The main contributions of the paper are elaborated below.

1) The hysteretic nonlinearities and dynamic uncertainties in PEA system are disposed explicitly and strictly via ADRC, so complicated identification of detailed hysteresis model and enormous calculation of its direct inverse model is not needed.
2) The sample-data CILC law is simple and can be implemented in a relatively easy manner, since it is designed on the basis of a linear second-order PEA model after using ADRC to compensate for hysteresis.
3) The effectiveness and robustness of the CILC guarantee that incomplete compensation of hysteresis will not deteriorate the tracking precision.
4) The control performance and applicability of the whole strategy have been substantiated by comparative experiments for different reference trajectories with multiple shapes and multiple frequencies including continuous and discontinuous, smooth and non-smooth, low-frequency and high-frequency signals.

The rest of the paper is organized as follows. A SODB model of PEA is developed in Section II. ADRC method with hysteresis compensation is given in Section III. In Section IV, in order to further decrease the tracking errors, a sampled-data CILC loop is incorporated to previous controller, and its rigorous convergence analysis is presented. Afterwards, comparative experiments are provided to verify the feasibility of the proposed strategy in Section V. Finally, Section VI concludes this paper.

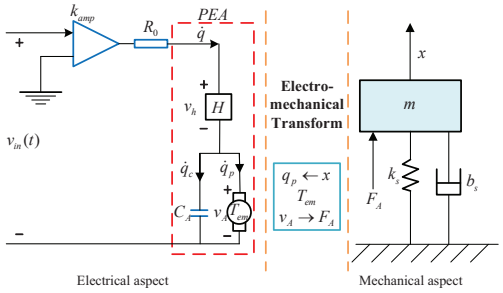

Fig. 1. The integrated dynamic model of the PEA.

II. Formulation of PEA's SODB Model

PEA commonly is composed of piezoelectric-driven ceramics material and nano-positioning machinery. As shown in Fig. 1, an integrated dynamic model [23] of the PEA which involves electrical and mechanical components is introduced

to describe the complex relations included in the PEA [4]. Then, by reformulating the integrated dynamic model of PEA, a SODB model is obtained. More specifically, the integrated dynamic model of the PEA is introduced in [23] as

$$R_0\dot{q}(t) + v_h(t) + v_A(t) = k_{amp}v_{in}(t) \quad (1)$$
$$v_h(t) = H(q) \quad (2)$$
$$q(t) = q_c(t) + q_p(t) \quad (3)$$
$$v_A(t) = q_c(t)/C_A \quad (4)$$
$$q_p(t) = T_{em}x(t) \quad (5)$$
$$F_A = T_{em}v_A(t) \quad (6)$$
$$m\ddot{x}(t) + b_s\dot{x}(t) + k_s x(t) = F_A. \quad (7)$$

The descriptions of the formulaic terms are given in Table I.

TABLE I
DESCRIPTIONS OF THE FORMULAIC TERMS.

Term	Description
R_0	Total resistances of driving circuits
q, $\dot{q}$	Charges and generating currents streaming in circuit of PEA
H	Hysteresis effects
v_h	Voltages produced by H
v_A	Transduced voltages
k_{amp}	Set ratio of piezoelectric ceramic servo power amplifier
$v_{in}(t)$	Input voltages to driving amplifier
C_A	General capacitances of piezoelectric ceramics in PEA
q_c	Charges stored in C_A
q_p	Transduced charges due to piezoelectric effects
T_{em}	Electromechanical transducer due to piezoelectric effects
x	Output displacements of PEA
F_A	Transduced forces
k_s, b_s, m	Stiffness coefficient, damping coefficient, and equivalent mass of positioning mechanism

With rearrangement, substituting (2)-(5) into (1) and (3)-(6) into (7) leads to (8) and (9), respectively, as follows:

$$R_0C_A\dot{q}(t) + q(t) - T_{em}x(t) = C_Ak_{amp}\left[v_{in}(t) - \frac{H(q)}{k_{amp}}\right] \quad (8)$$

$$m\ddot{x}(t) + b_s\dot{x}(t) + \left(k_s + \frac{T_{em}^2}{C_A}\right)x(t) = \frac{T_{em}}{C_A}q(t). \quad (9)$$

$R_0 = 0$ is assumed since any other external load is not considered [23]. Thus, after substituting (8) into (9), the integrated dynamic model is further simplified as

$$m\ddot{x}(t) + b_s\dot{x}(t) + k_s x(t) = T_{em}[k_{amp}v_{in}(t) - H(q)]. \quad (10)$$

The alleged parallel model which is introduced in [17] is shown in Fig. 2, where the hysteretic effect H is treated as a disturbance which is generated from the output displacements

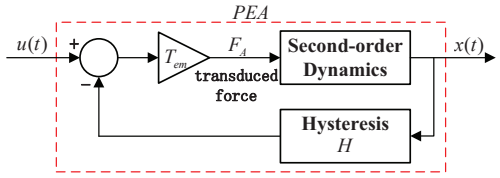

Fig. 2. The parallel structure of the PEA.

to the input voltages. Such a generic paradigm of modelling [24] is gained from (10). As shown in Fig. 3, (10) is reformulated as a SODB model via using the ADRC method. Subsequently, (10) is represented as

$$\ddot{x}(t) = f(\cdot) + bu(t) \quad (11)$$

where b represents a coefficient to adjust the control effort, $f(\cdot)$ is a disturbance which contains the hysteretic effect and other dynamic nonlinearity, and $u(t) = k_{amp}v_{in}(t)$.

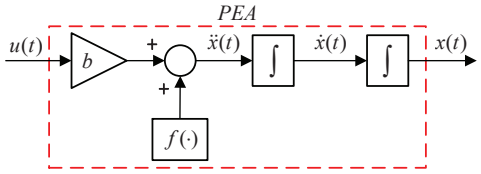

Fig. 3. The SODB model of the PEA.

Neither the hysteresis model nor its inversion is required when applying the SODB model (11). Then, the disturbance term $f(\cdot)$ can be estimated in real time by utilizing a LESO so that (11) comes close to the EDI model. Thus, a pure PI control algorithm is selected to control the EDI model.

III. HYSTERESIS COMPENSATION VIA ADRC

The original active disturbance rejection controller includes three components which are control law, extended state observer (ESO), and tracking differentiator (TD). Nevertheless, as shown in Fig. 4, the TD is not utilized in the proposed approach. The main idea of the proposed scheme is straightforward: the hysteresis $f(\cdot)$ of PEA is estimated by using the LESO, and compensated by designing the control law.

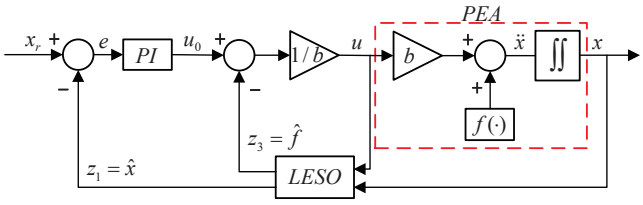

Fig. 4. The schematic structure of the proposed ADRC method.

A. LESO

The primary ESO which was firstly proposed in [25] shows chattering phenomena and is difficult to implement in actual applications since it is a typical nonlinear observer. Therefore, it was simplified as a LESO in [26] to overcome its limitations. The LESO which is used in the proposed approach defines an extended state space where disturbance term $f(\cdot)$ is regarded as an augmented state variable to be estimated. Afterwards, the SODB model (11) can be rewritten as the following state space model with $x = [x_1, x_2, x_3]^T = [x, \dot{x}, f]^T$ and $h = \dot{f}$:

$$\dot{x} = Ax + Bu + Eh$$
$$y = Cx \quad (12)$$

where $A = \begin{bmatrix} 0 & 1 & 0 \\ 0 & 0 & 1 \\ 0 & 0 & 0 \end{bmatrix}$, $B = \begin{bmatrix} 0 \\ b \\ 0 \end{bmatrix}$, $E = \begin{bmatrix} 0 \\ 0 \\ 1 \end{bmatrix}$, $C = \begin{bmatrix} 1 & 0 & 0 \end{bmatrix}$. Then, the extended state variable $f(\cdot)$ can be estimated in real-time by using a LESO in the following form

$$\begin{aligned} \dot{z} &= Az + Bu + L(y - \hat{y}) \\ \hat{y} &= Cz \end{aligned} \tag{13}$$

where $z = [z_1, z_2, z_3]^T = [\hat{x}, \hat{\dot{x}}, \hat{f}]$, $\hat{x}$, $\hat{\dot{x}}$, $\hat{f}$ are the estimated values of x, $\dot{x}$, f respectively, and $L = [\beta_1, \beta_2, \beta_3]^T$ is the observer gains vector.

The capabilities of LESO for estimating uncertainties have been analysed in S-domain in [27], where LESO not only shows excellent convergence, but also achieves accurate estimation of state variables as well as general disturbance, no matter whether f is bounded and known or not. The convergence and estimation capabilities of LESO in Z-domain are summarized as follows.

Lemma 1: Assume that the system is stable, and $U(z)$ and $X(z)$ are bounded. Then by defining the estimation errors: $\tilde{e} = [\tilde{e}_1, \tilde{e}_2, \tilde{e}_3]^T = x - z$, the final value of estimation error is given by

$$\lim_{k\to\infty} \tilde{e}(k) = \lim_{z\to 1} \frac{z-1}{z} \tilde{e}_i(z) = 0, \quad i = 1, 2, 3 \tag{14}$$

where $\tilde{e}(k)$ is the estimation errors of the kth sampling.

B. Control Law

After the estimate of the disturbance term $f(\cdot)$ is obtained from the LESO, the control law can be devised as

$$u = \frac{u_0 - z_3}{b}, \tag{15}$$

Substituting it into (11) gives

$$\ddot{x} = (f - z_3) + u_0 \approx u_0 \tag{16}$$

so that the EDI model (16) has been obtained. After that, multiple control schemes can be selected to achieve desired tracking performances. In the proposed method, a pure PI controller is used to readily control the EDI model of PEA:

$$u_0 = K_p(x_r - z_1) + K_i \int (x_r - z_1)dt \tag{17}$$

where K_p and K_i represent the gains of the pure PI controller.

IV. Sampled-Data CILC

A novel control scheme which combines CILC and ADRC is presented to achieve higher-performance tracking control of PEA systems. For the discrete-time implementation, we first get the continuous-time S-domain expression of (11) by applying Laplace transform. After that, by using Z-transform with a sampling time T_s and the zero-order hold, the Z-domain expression of (11) can be obtained as follows:

$$X(z) = \frac{T_s z}{(z-1)^2}[f(z) + bU(z)]. \tag{18}$$

The time duration $[0, T]$ is finite and discretized in a set $\mathcal{N}$ with sampling points $0, 1, \cdots, N$, where $T = NT_s > 0$. The main control goal is to track the given trajectory $x_r(k), \forall k \in \mathcal{N}$.

A. Structure of Sampled-data CILC

As seen from Fig. 5, the sampled-data CILC law combining ADRC for PEA systems is defined in the Z-domain as

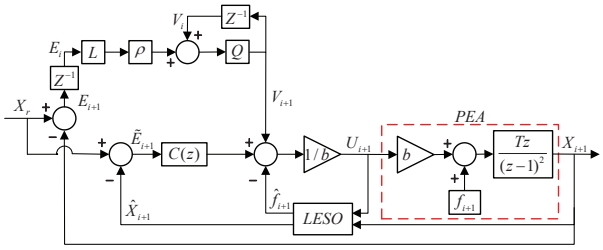

Fig. 5. The schematic block diagram of CILC combined with ADRC, where $C(z)$, ρ, Q, and L are the PI controller, learning gain, Q-filter, and learning filter, respectively. The operator Z^{-1} denotes one iteration backward shift.

$$U_{i+1}(z) = [C(z)\tilde{E}_{i+1}(z) + V_{i+1}(z) - \hat{f}_{i+1}(z)]/b \tag{19}$$

where $U_{i+1}(z)$, $\tilde{E}_{i+1}(z) = X_r(z) - \hat{X}_{i+1}(z)$ and $\hat{f}_{i+1}(z)$ are the control input of PEA system, the estimated output tracking errors and the general disturbance at the $(i+1)$th iteration, respectively, and $C(z)$ is the pure PI control function. In (19), $V_{i+1}(z)$ which represents the output of the ILC part that is included in CILC satisfies

$$V_{i+1}(z) = Q(z)[V_i(z) + \rho L(z)E_i(z)] \tag{20}$$

where $L(z)$ and $Q(z)$ are the learning filter and Q-filter, and $E_i(z) = X_r(z) - X_i(z)$ represents the measured output tracking error. Besides, ρ is a time-varying positive learning coefficient. Since $V_{i+1}(z)$ is computed from control input $V_i(z)$ and tracking errors output $E_i(z)$ in the last iteration, the ILC law (20) is a feedforward control strategy obviously.

Let us consider a case that PEA positioning system after ADRC compensation has been stabilized by the pure PI controller $C(z)$ and the reference $X_r(z)$ only includes frequencies up to the bandwidth frequency ω_b rad/s which are below the Nyquist frequency ω_s rad/s. Moreover, ω_c rad/s defines the cutoff frequency which is selected for $Q(z)$ in the range $\omega_s > \omega_c > \omega_b$. The interval is defined as $\mathcal{I} = [-\omega_c T_s, \omega_c T_s]$. The convergence analysis results of the CILC law (19) and (20) are summarized in the following theorem.

Theorem 1: If ρ, $Q(z)$, and $L(z)$ are devised as

$$\zeta = \sup_{\theta\in\mathcal{I}} \left| Q(e^{j\theta}) \left[1 - \rho L(e^{j\theta})P(e^{j\theta})\right] \right| < 1 \tag{21}$$

where $P(z) = T_s z/[T_s z C(z) + (z-1)^2]$, the CILC laws (19) and (20) can ensure that

$$\lim_{i\to\infty} \sup_{\theta\in\mathcal{I}} \left| E_i(e^{j\theta}) \right| \le \Xi_1 + \Xi_2\delta_1 + \Xi_3\delta_2 \tag{22}$$

where δ_1, δ_2 are positive constants and

$$\begin{aligned} \Xi_1 &= \frac{1}{1-\zeta} \sup_{\theta\in\mathcal{I}} \left| S(e^{j\theta}) \left[1 - Q(e^{j\theta})\right] X_r(e^{j\theta}) \right| \\ \Xi_2 &= \frac{\rho}{1-\zeta} \sup_{\theta\in\mathcal{I}} \left| Q(e^{j\theta}) L(e^{j\theta}) P^2(e^{j\theta}) C(e^{j\theta}) \right| \\ &\quad + \sup_{\theta\in\mathcal{I}} \left| P(e^{j\theta}) C(e^{j\theta}) \right| \\ \Xi_3 &= \frac{\rho}{1-\zeta} \sup_{\theta\in\mathcal{I}} \left| Q(e^{j\theta}) L(e^{j\theta}) P^2(e^{j\theta}) \right| + \sup_{\theta\in\mathcal{I}} \left| P(e^{j\theta}) \right| \end{aligned}$$

where $S(z) = (z-1)^2/[T_s z C(z) + (z-1)^2]$.

Proof: See Appendix.

B. Selection of Q(z)

The learning convergence condition (21) gained for CILC law implies that the Nyquist plots of the term $Q(z)[1 - \rho L(z)P(z)]$ must be inside a unit circle and centered at the origin of the complex plane. The learning convergence condition (21) can be met by correct choices of ρ, $L(z)$, and $Q(z)$. However, it is worth noting from (31) that the tracking errors $E(z)$ will be influenced by $X_r(z)$ via an element $S(z)[1 - Q(z)]$. Thus, the selection of $Q(z)$ should give consideration to that

$$\sup_{\theta \in \mathcal{I}} \left| S(e^{j\theta}) \left[1 - Q(e^{j\theta})\right] \right| \ll 1 \tag{23}$$

in order to minimize the tracking errors $E(z)$. The condition (23) means that the term $1 - Q(z)$ must be close to zero as much as possible so as to depress the steady-state error which may happen by using filter $Q(z)$. The counterpart to the condition (21) is given as follows:

$$\left|1 - \rho L(e^{j\theta}) P(e^{j\theta})\right| < \frac{1}{|Q(e^{j\theta})|}, \quad \theta \in \mathcal{I}. \tag{24}$$

A remarkable advantage which can be seen from (24) is that the stable region for certain frequencies will be enlarged when the gain of filter $Q(z)$ is less than one.

C. Selection of L(z)

For the selection of $L(z)$, different choices would lead to different classes of ILC scheme in CILC law, e.g., P-type ILC $L(z) = 1$, D-type ILC $L(z) = 1 - z^{-1}$, and D^2-type ILC $L(z) = 1 - 2z^{-1} + z^{-2}$ [28]. In particular, if the PI controller $C(z)$ is predetermined, $P(z)$ is obtainable for the ILC scheme in CILC law design. Therefore, when $P(z)$ is minimum phase, the learning filter $L(z)$ can be set to be the inversion of $P(z)$, namely $L(z) = P^{-1}(z)$. After that, the learning gain ρ can be fixed on $\rho = 1$ leading to the fastest convergence speed on the basis of (31), namely $1 - \rho L(z)P(z) = 0$.

V. Experimental Comparisons and Discussions

Experiments are carried out on a PEA system to imply the control performance of the proposed approach for three different reference signals $y_r(t)$ with multiple shapes and multiple frequencies including continuous and discontinuous, smooth and non-smooth, low-frequency and high-frequency signals. More specifically, 10, 50, 100, and 200 Hz polynomial curve, 100 and 200 Hz triangular wave and step signal are handled. For illustration, the 10 Hz polynomial curve is defined as

$$y_r(t) = \frac{4}{0.05^6} t^3 (0.1 - t)^3 \mu m, \quad t \in [0, 0.1] s. \tag{25}$$

For abbreviation, *Cases* 1-8 represent tracking of 10 Hz polynomial curve, 50 Hz polynomial curve, 100 Hz polynomial curve, 200 Hz polynomial curve, 100 Hz triangular wave, 200 Hz triangular wave, 100 Hz step signal, as well as 200 Hz step signal, respectively. The tracking precision is assessed through RMSE, RE, and MAE, which are given as

$$RMSE = \sqrt{\sum_{i=1}^{N} (y_i - y_r)^2 / N} \tag{26}$$

$$RE = \sqrt{\sum_{i=1}^{N} (y_i - y_r)^2 / \sum_{i=1}^{N} y_r^2} \tag{27}$$

$$MAE = \sup |y_i - y_r| \tag{28}$$

where y_r is the reference signal, y_i is the output of the PEA, and N is the total number of data.

A. Experimental Setup

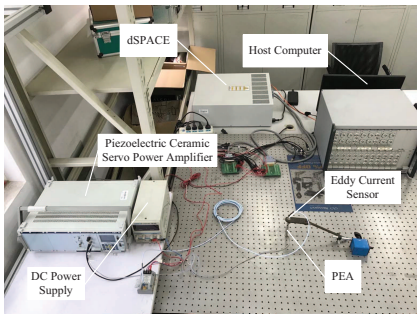

(a) The experimental platform.

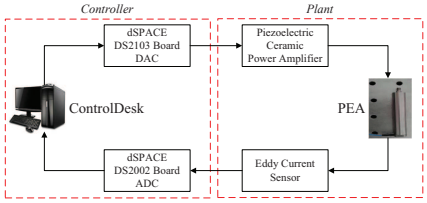

(b) The block diagram of the whole system.

Fig. 6. The experimental setup.

The corresponding experimental platform and block diagram of the whole system are shown in Fig. 6. The PEA nano-positioning system is built on a M-ST-46-8 SMART TABLES optical vibration isolation platform bought from Newport Corporation. It is used to separate oscillation, attrition, and external disturbances. A PSt150/7/60VS12 PEA which is produced by Harbin Core Tomorrow Science and Technology Co., Ltd is utilized for testing. It is able to move 63.69 μm in X and Y directions. An eddy current sensor which is used to measure the output displacements of PEA is integrated in the positioning system. A piezoelectric ceramic servo power amplifier is connected to the system to drive PEA. The designed control strategies are conducted by MATLAB/SIMULINK to create and send C codes to a dSPACE DS1006 board which is utilized to communicate the input voltage signals and output displacements between the PEA and host computer. Two boards DS2103 and DS2002 are used as 32×14-bits digital-analog converter (DAC) with 10 μs conversion time and 32×16-bits analog-digital converter (ADC) with 5 μs settling time. The input voltages of DAC channel and ADC channel are between $\pm 10\, V$. The parameters of the designed controller can be tuned through the Real-Time Workshop and ControlDesk Human-Computer Interface so

that the control performance can be validated via the intuitive experimental results in real time. The sampling cycle is chosen as 0.1 ms throughout the process.

B. Pure PI Control

In this part, a pure PI control law is defined as

$$C(s) = K_p + \frac{K_i}{s} \tag{29}$$

where K_i and K_p are the integral and proportional coefficients. The Ziegler-Nicholes means [29] is adopted to obtain the best tracking performances. The tuned parameters and tracking precision in the situation of eight different-type trajectories are listed in Table II. It is worth noting that the absolute tracking error becomes large at certain positions owing to the discontinuity of the step signals. This results in the MAE inadequate in judging the control performances of PEA for the remaining continuous parts, and thus omitted here. The control performances of PEA utilizing pure PI control with 8 cases are shown in Fig. 7. These intuitive profiles reveal that

TABLE II
TRACKING PRECISION OF PEA SYSTEM UTILIZING PURE PI CONTROL.

Case	K_p, K_i	RMSE/nm	RE/%	MAE/nm
1	0.5, 1100	59.8	1.46	97.7
2	0.75, 1950	74.6	1.82	124.6
3	1.15, 2100	99.4	2.42	163.1
4	0.95, 2250	156.0	3.80	250.9
5	1.2, 2000	135.8	3.26	189.9
6	1.1, 2100	240.8	5.91	350.1
7	0.4, 850	410.1	14.47	
8	0.25, 900	621.9	21.91	

- There are bigger phase retardation between the desired trajectories and the practical displacements when the frequency of references becomes higher;
- The control precision is degraded with the increase of references' frequency;
- Higher PI parameters are required to obtain the possible best tracking performances when the references get higher frequency.

Pure PI control achieves good control performance in tracking low-frequency smooth references (10, and 50 Hz polynomial curves), but fails to get a satisfying tracking precision due to the rate-dependent characteristics of hysteresis when the frequency of references is high. Furthermore, the control performance becomes worse when either non-smooth (triangular wave) references or discontinuous (step signal) trajectories are employed than that when smooth (polynomial curve) signals are adopted.

C. ADRC

ADRC based upon the SODB mode of PEA is further designed. By several trial-and-error processes, the observer parameters of the LESO are set as $L = [\beta_1, \beta_2, \beta_3]^T = [5000, 5500, 250]^T$. Subsequently, the coefficients of control law (15) are tuned with the gains of the LESO determined. For a fair comparison, the gains of the pure PI control strategy in (17) are fixed to be the same as the parameters set in (29). Another gain b is selected to be $b = 4$.

Results of control performances are listed in Table III. Fig. 8 suggests the control performances of the PEA employing ADRC in tracking 8 different references trajectories. From these experimental results we can see that

TABLE III
TRACKING PRECISION OF PEA SYSTEM UTILIZING ADRC. IM.: IMPROVEMENT OF TRACKING PRECISION RELATIVE TO PURE PI CONTROL.

Case	RMSE/nm	Im./%	RE/%	Im./%	MAE/nm	Im./%
1	26.5	55.69	0.65	55.48	50.5	48.31
2	25.9	65.28	0.63	65.38	59.9	51.93
3	30.5	69.32	0.74	69.42	71.3	56.28
4	42.4	72.82	1.03	72.89	92.2	63.25
5	36.0	73.49	0.86	73.62	88.6	53.34
6	45.1	81.27	1.08	81.73	97.1	72.27
7	347.1	15.36	12.25	15.34		
8	526.0	15.42	18.53	15.43		

- The MAE, RE, and RMSE are significantly reduced at least 48.31% relative to the pure PI control in cases 1-5, although they are less reduced in cases 7 and 8;
- Higher frequency accompanies larger precision improvement in terms of the tracking error and control performance;
- Acceptable tracking precision is obtained when either non-smooth (triangular wave) references or discontinuous (step signal) trajectories are given.

The profiles demonstrate that the ADRC stratery is better than the pure PI control method. However, there is still a possibility of further improvement regarding the tracking precision and control error.

D. CILC via ADRC for Hysteresis Compensation

In this part, the CILC law (19) with ADRC solution for hysteresis compensation are exploited for PEA to perform the given tracking tasks, where the reference trajectories are the same as in ADRC and the pure PI control. Then, we consider the selection of the learning gain ρ, the learning filter $L(z)$, and the Q-filter $Q(z)$. For the reason that the poles and zeros of $P(z)$ are all inside the unit circle and the PI controller $C(z)$ stabilizes the system after ADRC compensating for hysteresis, the learning filter $L(z)$ is selected to be $L(z) = P^{-1}(z)$. Furthermore, according to (31), the learning gain is fixed on $\rho = 1$ to guarantee the fastest convergence rate. The incomplete part is to choose $Q(z)$. The zero-phase filter is designed with a finite impulse response (FIR) method for $Q(z)$ to filter out any possible external noise in the output channels. More specifically, the MATLAB function *designfilt* with setting the normalized passband and stopband frequency (0.01π $rad/sample$ and 0.05π $rad/sample$ for 10 Hz references; 0.03π $rad/sample$ and 0.1π $rad/sample$ for 50 and 100 Hz references; 0.04π $rad/sample$ and 0.2π $rad/sample$ for 200 Hz references) is utilized to produce a low-pass filter ω which is applied by the MATLAB function *filtilt*(ω, y_i) to filter the measured output displacement of PEA y_i.

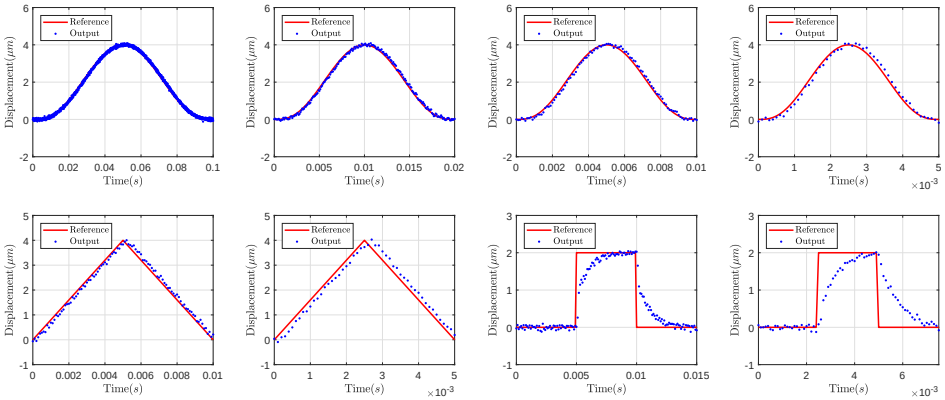

Fig. 7. Tracking performances of PEA system utilizing pure PI control. Top first: polynomial curve (10 Hz), top second: polynomial curve (50 Hz), top third: polynomial curve (100 Hz), top fourth: polynomial curve (200 Hz), bottom first: triangular wave (100 Hz), bottom second: triangular wave (200 Hz), bottom third: step signal (100 Hz), and bottom fourth: step signal (200 Hz).

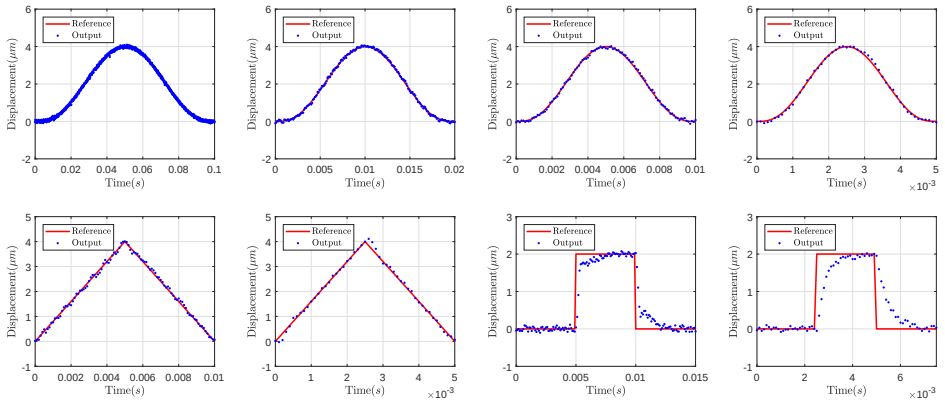

Fig. 8. Tracking performances of PEA system utilizing ADRC. Top first: polynomial curve (10 Hz), top second: polynomial curve (50 Hz), top third: polynomial curve (100 Hz), top fourth: polynomial curve (200 Hz), bottom first: triangular wave (100 Hz), bottom second: triangular wave (200 Hz), bottom third: step signal (100 Hz), and bottom fourth: step signal (200 Hz).

In the experiments, ADRC solution for hysteresis compensation is conducted before the initial trial of CILC. The control input generated by ADRC is used as V_0 in (20). Then, by utilizing the information of input and output in the last iteration to update the control input iteratively, the proposed method is implemented. Figs. 9-11 give the experimental results of RMSE, RE, and MAE. The control performance of PEA in tracking step signals is shown in Fig. 12. We can find that

- Not only for smooth (polynomial curve) signals but also for non-smooth (triangular wave) references and even for discontinuous (step signal) trajectories, the tracking accuracy has been improved remarkably within 6 iterations on the basis of ADRC solution for hysteresis compensation;
- The CILC scheme expedites the convergence speed, and a dominant improvement of the tracking accuracy after the first iteration is achieved;
- For 10, 50, and 100 Hz polynomial curve references, the final MAE of tracking performance via ILC almost drops to the level of hardware limitation;
- For non-smooth (triangular wave) references, though the RMSE and RE do not decrease monotonically in the iteration domain, it still shows a downward trend during the whole process;
- For discontinuous (step signal) trajectories, CILC scheme still improves the tracking accuracy by 27.28% (100 Hz) and 35.13% (200 Hz).

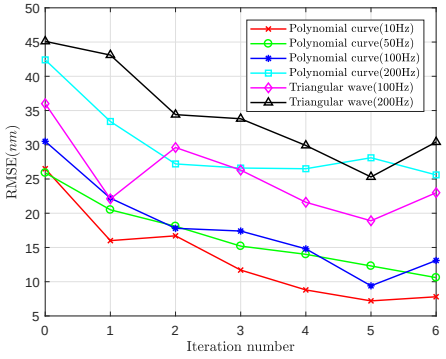

Fig. 9. RMSE profile of tracking performances via CILC.

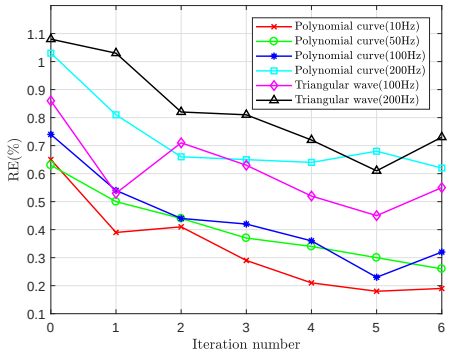

Fig. 10. RE profile of tracking performances via CILC.

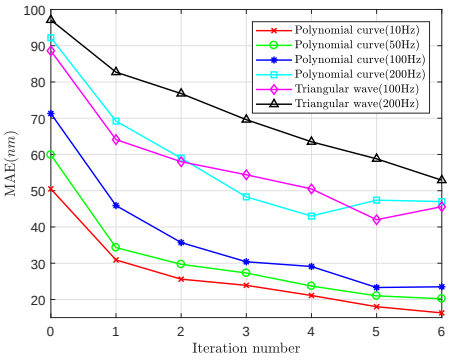

Fig. 11. MAE profile of tracking performancess via CILC.

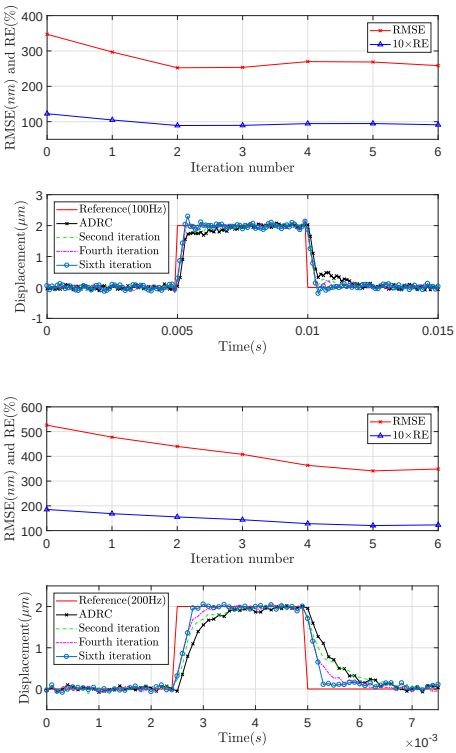

Fig. 12. The CILC performances in tracking step signal.

In summary, compared with pure PI and ADRC with hysteresis compensation, satisfactory tracking performance is obtained, and the incorporation of CILC and ADRC shows tremendous superiority in addressing high-precision tracking tasks for PEA system.

VI. Conclusion

In this paper, a SODB model of the PEA is proposed. Meanwhile, the LESO is used to estimate the hysteresis which is treated as a general disturbance so that neither the hysteresis model nor its inversion is needed. An innovative control method which combines CILC and ADRC is proposed to address the high-precision position tracking problems which are found in PEA systems, and the learning convergence condition of CILC is derived rigorously. Comparative experiments are executed to verify the merits of the proposed strategy. Results illustrate that the control performances are enhanced tremendously not only for smooth (polynomial curve) signals, but also for non-smooth (triangular wave) references and even for discontinuous (step signal) trajectories. It shows better performance than ADRC scheme and pure PI control method according to control performance and tracking error, and it is an efficacious scheme to settle the control issue produced by the rate-dependent hysteretic nonlinearity of high-precision PEA positioning systems.

Appendix
Proof of the Theorem 1

For abbreviation, the term z is omitted in following derivation processes. From Fig. 5, we can get

$$E_{i+1} = X_r - X_{i+1} = X_r - \frac{T_s z}{(z-1)^2}(f_{i+1} + bU_{i+1}). \quad (30)$$

Substituting (19) into (30) and rearrangement leads to

$$E_{i+1} = SX_r - P[V_{i+1} + C(X_{i+1} - \hat{X}_{i+1}) + (f_{i+1} - \hat{f}_{i+1})]. \quad (31)$$

In the ith iteration, (31) gives

$$-PV_i = E_i - SX_r + PC(X_i - \hat{X}_i) + P(f_i - \hat{f}_i). \quad (32)$$

In the meantime, multiplying by term $-P$ on both sides of (20) gives

$$-PV_{i+1} = -QPV_i - \rho LPQE_i. \quad (33)$$

By substituting (32) into (33), we have

$$\begin{aligned} -PV_{i+1} &= Q[E_i - SX_r + PC(X_i - \hat{X}_i) \\ &\quad + P(f_i - \hat{f}_i)] - \rho LPQE_i \\ &= \varpi E_i - SQX_r + PQC(X_i - \hat{X}_i) + PQ(f_i - \hat{f}_i) \end{aligned} \quad (34)$$

where $\varpi = Q(1-\rho LP)$. Afterwards, by substituting (34) into (31), we can derive the relation of tracking error between two successive iterations which follows that

$$\begin{aligned} E_{i+1} &= \varpi E_i + S(1-Q)X_r \\ &\quad - PC(X_{i+1} - \hat{X}_{i+1}) + PQC(X_i - \hat{X}_i) \\ &\quad - P(f_{i+1} - \hat{f}_{i+1}) + PQ(f_i - \hat{f}_i). \end{aligned} \quad (35)$$

By employing (35) repeatedly, it yields

$$\begin{aligned}E_{i+1} = {} & \varpi^i E_1 + S(1-Q)X_r \sum_{j=0}^{i-1} \varpi^j \\ & - PC \sum_{j=0}^{i-1} \varpi^j (X_{i+1-j} - \hat{X}_{i+1-j}) \\ & + PQC \sum_{j=0}^{i-1} \varpi^j (X_{i-j} - \hat{X}_{i-j}) \\ & - P \sum_{j=0}^{i-1} \varpi^j (f_{i+1-j} - \hat{f}_{i+1-j}) \\ & + PQ \sum_{j=0}^{i-1} \varpi^j (f_{i-j} - \hat{f}_{i-j}). \end{aligned} \tag{36}$$

Rewriting the fourth and sixth terms on the right-hand side of (36) gives

$$\begin{aligned} & PQC \sum_{j=0}^{i-1} \varpi^j (X_{i-j} - \hat{X}_{i-j}) \\ & = (Q-\varpi)PC \sum_{j=0}^{i-1} \varpi^j (X_{i-j} - \hat{X}_{i-j}) \\ & \quad + PC \sum_{j=0}^{i-1} \varpi^{j+1} (X_{i-j} - \hat{X}_{i-j}) \\ & = \rho QLP^2 C \sum_{j=0}^{i-1} \varpi^j (X_{i-j} - \hat{X}_{i-j}) \\ & \quad + PC \sum_{j=1}^{i} \varpi^j (X_{i+1-j} - \hat{X}_{i+1-j}) \end{aligned} \tag{37}$$

and

$$\begin{aligned} & PQ \sum_{j=0}^{i-1} \varpi^j (f_{i-j} - \hat{f}_{i-j}) \\ & = (Q-\varpi)P \sum_{j=0}^{i-1} \varpi^j (f_{i-j} - \hat{f}_{i-j}) + P \sum_{j=0}^{i-1} \varpi^{j+1} (f_{i-j} - \hat{f}_{i-j}) \\ & = \rho QLP^2 \sum_{j=0}^{i-1} \varpi^j (f_{i-j} - \hat{f}_{i-j}) + P \sum_{j=1}^{i} \varpi^j (f_{i+1-j} - \hat{f}_{i+1-j}) \end{aligned} \tag{38}$$

respectively. Substituting (37) and (38) into (36) induces

$$\begin{aligned} E_{i+1} = {} & \varpi^i E_1 + S(1-Q)X_r \sum_{j=0}^{i-1} \varpi^j \\ & + \rho QLP^2 C \sum_{j=0}^{i-1} \varpi^j (X_{i-j} - \hat{X}_{i-j}) \\ & + PC\varpi^i (X_1 - \hat{X}_1) - PC(X_{i+1} - \hat{X}_{i+1}) \\ & + \rho QLP^2 \sum_{j=0}^{i-1} \varpi^j (f_{i-j} - \hat{f}_{i-j}) \\ & + P\varpi^i (f_1 - \hat{f}_1) - P(f_{i+1} - \hat{f}_{i+1}). \end{aligned} \tag{39}$$

Then, taking absolute values on both sides of (39) implies

$$\begin{aligned} |E_{i+1}| \le {} & |\varpi|^i |E_1| + |S(1-Q)X_r| \sum_{j=0}^{i-1} |\varpi|^j \\ & + |\rho QLP^2 C| \sum_{j=0}^{i-1} |\varpi|^j |X_{i-j} - \hat{X}_{i-j}| \\ & + |PC||\varpi|^i |X_1 - \hat{X}_1| + |PC||X_{i+1} - \hat{X}_{i+1}| \\ & + |\rho QLP^2| \sum_{j=0}^{i-1} |\varpi|^j |f_{i-j} - \hat{f}_{i-j}| \\ & + |P||\varpi|^i |f_1 - \hat{f}_1| + |P||f_{i+1} - \hat{f}_{i+1}|. \end{aligned} \tag{40}$$

Noticing that $\sup_{\theta\in\mathcal{I}} |\varpi(e^{j\theta})| = \zeta$ is given by (21) and that the estimated error can be considered as bounded in the finite sampled instances, namely, $\sup_{\theta\in\mathcal{I}} |X_i(e^{j\theta}) - \hat{X}_i(e^{j\theta})| < \delta_1$ and $\sup_{\theta\in\mathcal{I}} |f_i(e^{j\theta}) - \hat{f}_i(e^{j\theta})| < \delta_2$ by applying *Lemma 1*, we further have

$$\begin{aligned} \sup_{\theta\in\mathcal{I}} |E_{i+1}| \le {} & \zeta^i \sup_{\theta\in\mathcal{I}} |E_1| + \sup_{\theta\in\mathcal{I}} |S(1-Q)X_r| \frac{1-\zeta^{i-1}}{1-\zeta} \\ & + \rho\delta_1 \sup_{\theta\in\mathcal{I}} |QLP^2 C| \frac{1-\zeta^{i-1}}{1-\zeta} \\ & + \sup_{\theta\in\mathcal{I}} |PC| \zeta^i \delta_1 + \sup_{\theta\in\mathcal{I}} |PC| \delta_1 \\ & + \rho\delta_2 \sup_{\theta\in\mathcal{I}} |QLP^2| \frac{1-\zeta^{i-1}}{1-\zeta} \\ & + \sup_{\theta\in\mathcal{I}} |P| \zeta^i \delta_2 + \sup_{\theta\in\mathcal{I}} |P| \delta_2. \end{aligned} \tag{41}$$

Since PEA system has been stabilized by the PI controller C after ADRC compensation in the first iteration, $\sup_{\theta\in\mathcal{I}} |E_1|$ is a finite value. In addition, $0 \le \zeta < 1$ means that $\lim_{i\to\infty} \zeta^i = 0$. Hence

$$\begin{aligned} \lim_{i\to\infty} \sup_{\theta\in\mathcal{I}} |E_{i+1}| \le {} & \frac{1}{1-\zeta} \sup_{\theta\in\mathcal{I}} |S(1-Q)X_r| \\ & + \left(\frac{\rho}{1-\zeta} \sup_{\theta\in\mathcal{I}} |QLP^2 C| + \sup_{\theta\in\mathcal{I}} |PC| \right) \delta_1 \\ & + \left(\frac{\rho}{1-\zeta} \sup_{\theta\in\mathcal{I}} |QLP^2| + \sup_{\theta\in\mathcal{I}} |P| \right) \delta_2. \end{aligned} \tag{42}$$

With the definitions Ξ_i, $i = 1, 2$, the proof is completed.

REFERENCES

[1] Y. Li and Q. Xu, "A novel piezoactuated XY stage with parallel, decoupled, and stacked flexure structure for micro/nanopositioning," *IEEE Trans. Ind. Electron.*, vol. 58, no. 8, pp. 3601–3615, Aug. 2011.

[2] I. Grinberg, N. Maccabi, and D. Elata, "A pure-twisting piezoelectric actuator for tilting micromirror applications solid-state sensors," in *Proc. 2017 Int. Conf. Solid-State Sens., Actuators Microsyst.*, Kaohsiung, Taiwan, Jun. 2017, pp. 18–22.

[3] M. Kozek, C. Benatzky, A. Schirrer, and A. Stribersky, "Vibration damping of a flexible car body structure using piezo-stack actuators," *Control Eng. Pract.*, vol. 19, no. 3, pp. 298–310, Mar. 2011.

[4] G.-Y. Gu, L.-M. Zhu, C.-Y. Su, H. Ding, and S. Fatikow, "Modeling and control of piezo-actuated nanopositioning stages: a survey," *IEEE Trans. Autom. Sci. Eng.*, vol. 13, no. 1, pp. 313–332, Sep. 2016.

[5] Q. Xu, "Precision motion control of piezoelectric nanopositioning stage with chattering-free adaptive sliding mode control," *IEEE Trans. Autom. Sci. Eng.*, vol. 14, no. 1, pp. 238–248, Jan. 2017.

[6] Q. Xu, "Continuous integral terminal third-order sliding mode motion cntrol for piezoelectric nanopositioning system," *IEEE/ASME Trans. Mechatronics*, vol. 22, no. 4, pp. 1828–1838, Aug. 2017.

[7] X. Chen, C. Y. Su, Z. Li, and F. Yang, "Design of implementable adaptive control for micro/nano positioning system driven by piezoelectric actuator," *IEEE Trans. Ind. Electron.*, vol. 63, no. 10, pp. 6471–6481, 2016.

[8] A. Sebastian and S.M. Salapaka, "Design methodologies for robust nanopositioning," *IEEE Trans. Control Syst. Technol.*, vol. 13, no. 6, pp. 868–876, Nov. 2005.

[9] B. Jayawardhana, H. Logemann, and P. Ryan, "PID control of second-order systems with hysteresis," *Int. J. Control*, vol. 81, no. 8, pp. 1331–1342, Aug. 2008.

[10] X. Zhang and C. Su, "Adaptive Neural Network dynamic surface control for a class of time-delay nonlinear systems with hysteresis inputs and dynamic uncertainties," *IEEE Trans. Neural Netw. Learn. Syst.*, vol. 26, no. 11, pp. 2844–2860, Nov. 2015.

[11] H. Jiang, H. Ji, and J. Qiu, "A modified prandtl-ishlinskii model for modeling asymmetric hysteresis of piezoelectric actuators," *IEEE Trans. Ultrason., Ferroelect., Freq. Control*, vol. 57, no. 5, pp. 1200–1210, May. 2010.

[12] G. Wang, S. Wang, and F. Bai, "Modeling and identification of piezoelectric hysteresis by an asymmetric Bouc-Wen model," in *Proc. 36th Chin. Control Conf.*, Dalian, China, Jul. 2017, pp. 2000–2005.

[13] J. Liu and K. Zhou, "Neural networks based modeling and robust control of hysteresis," in *Proc. 35th Chin. Control Conf.*, Chengdu, China, Jul. 2016, pp. 3051–3056.

[14] J. Han, "Auto disturbances rejection controller and its applications," *Control Decis.*, vol. 13, no. 1, pp. 19–23, 1998, (in Chinese).

[15] S. Zhang, H. Li, and R. Schmidt, "Disturbance rejection control for vibration suppression of piezoelectric laminated thin-walled structures," *J. Sound and Vibration*, vol. 333, no. 5, pp. 1209–1223, Feb. 2014.

[16] F. J. Goforth and Z. Gao, "An active disturbance rejection control solution for hysteresis compensation," in *Proc. 2008 Amer. Control Conf.*, Seattle, USA, Jun. 2008, pp. 2202–2208.

[17] W. Liu, L. Cheng, Z.-G. Hou, and M. Tan, "An active disturbance rejection controller with hysteresis compensation for piezoelectric actuators," in *Proc. 2016 12th World Congr. Intell. Control Autom.*, Guilin, China, Jun. 2016, pp. 2148–2153.

[18] D. Min, D. Huang, and Y. Jian, "High-precision tracking of piezoelectric actuator using active disturbance rejection control," in *Proc. 2018 5th Int. Conf. Inf., Cybern., Comput. Social Syst.*, Hangzhou, China, Aug. 2018, pp:13–18.

[19] L. Liu, K. K. Tan, A. S. Putra, and T. H. Lee, "Compensation of hysteresis in piezoelectric actuator with iterative learning control," *J. Control Theory and Appl.*, vol. 8, no. 2, pp. 176–180, 2010.

[20] J.-X. Xu, D. Huang, V. Venkataramanan, and T. C. T. Huynh, "Extreme precise motion tracking of piezoelectric positioning stage using sampleddata iterative learning control," *IEEE Trans. Control Syst. Technol.*, vol. 21, no. 4, pp. 1432–1439, Jun. 2013.

[21] Y. Jian, D. Huang, J. Liu, and D. Min, "High-Precision Tracking of Piezoelectric Actuator Using Iterative Learning Control and Direct Inverse Compensation of Hysteresis," *IEEE Trans. Ind. Electron.*, vol. 66, no. 1, pp. 368–377, Jan. 2019.

[22] D. Huang, J.-X. Xu, V. Venkataramanan, and T. C. T. Huynh, "High performance tracking of piezoelectric positioning stage using currentcycle iterative learning control with gain scheduling," *IEEE Trans. Ind. Electron.*, vol. 61, no. 2, pp. 1085–1098, Mar. 2014.

[23] G.-Y. Gu, L.-M. Zhu, C.-Y. Su, and H. Ding, "Motion control of piezoelectric positioning stages: Modeling, controller design and experimental evaluation," *IEEE/ASME Trans. Mechatronics*, vol. 18, no. 5, pp. 1459–1471, May 2013.

[24] L. Riccardi, D. Naso, B. Turchiano, and H. Janocha, "Design of linear feedback controllers for dynamic systems with hysteresis," *IEEE Trans. Control Syst. Technol.*, vol. 22, no. 4, pp. 1268–1280, Jul. 2014.

[25] J. Han, "From PID to active disturbance rejection control," *IEEE Trans. Ind. Electron.*, vol. 56, no. 3, pp. 900–906, Mar. 2009.

[26] Z. Gao, "Scaling and parameterization based controller tuning," in *Proc. 2003 Amer. Control Conf.*, Denver, USA, Jun. 2003, pp. 4989–4996.

[27] D. Zhang, X. Yao and Q. Wu, "Frequency-domain characteristics analysis of linear active disturbance rejection control for second-order systems," in *Proc. 34th Chin. Control Conf.*, Hangzhou, China, Jul. 2016, pp. 53–58.

[28] K. Abidi and J.-X. Xu, "Iterative learning control for sampled-data systems: From theory to practice," *IEEE Trans. Ind. Electron.*, vol. 58, no. 7, pp. 3002–3015, Aug. 2011.

[29] K. Astrom and T. Hagglund, *PID Controllers: Theory, Design and Tuning*. 2nd ed. Research Triangle Park, NC, USA: ISA Publ., 1995.

Deqing Huang (M'10) received the B.S. and Ph.D. degrees with a major of applied mathematics from the Mathematical College, Sichuan University, Chengdu, China, in 2002 and 2007, respectively. He attended the Department of Electrical and Computer Engineering (ECE), National University of Singapore (NUS), Singapore, in 2006, where he received the second Ph.D. degree with a major in control engineering in 2011. From January 2010 to February 2013, he was a Research Fellow in the Department of Electrical and Computer Engineering of NUS. From March 2013 to January 2016, he was a Research Associate with the Department of Aeronautics, Imperial College London, London, U.K. In January 2016, he joined the Department of Electronic and Information Engineering, Southwest Jiaotong University, Chengdu, China as professor and department head.

His research interests lie in the areas of modern control theory, artificial intelligence and fault diagnosis as well as robotics.

Da Min received the B.Eng. degree of automation from the Qixin Honors School, Zhejiang SciTech University, Hangzhou, China, in 2016. He is currently working towards the M.Eng. degree in Control Science and Engineering at the School of Electrical Engineering, Southwest Jiaotong University, Chengdu, China.

His current research interests include precision motion control, active disturbance rejection control theory, hysteresis nonlinearity control, and iterative learning control theory.

Yupei Jian received the B.Eng. and M.Eng. degrees from the School of Electrical Engineering, Southwest Jiaotong University, China, in 2016 and 2019, respectively. He is currently working towards the Ph.D. degree in mechanical engineering at the University of Auckland, Auckland, New Zealand.

His current research interests lie in tunable metamaterials/metastructures, and the application of metamaterials for energy harvester design.

Yanan Li received the B.Eng. and M.Eng. degrees from the Harbin Institute of Technology, China, in 2006 and 2008, respectively, and the Ph.D. degree from the National University of Singapore, Singapore, in 2013. He is currently a Lecturer in control engineering with the Department of Engineering and Design, University of Sussex, Sussex, U.K. From 2015 to 2017, he was a Research Associate with the Department of Bioengineering, Imperial College London, London, U.K. From 2013 to 2015, he was a Research Scientist with the Institute for Infocomm Research, Agency for Science, Technology and Research, Singapore.

His general research interests include human-robot interaction, robot control and control theory and applications.